Luminescent Eu(III) hybrid materials for sensor applications†

Beatriz Carmen Barja* and Pedro Francisco Aramendía

In this work we use the sol–gel technique to develop different luminescent Eu(III) porous materials from a bis(trialkoxysilyl) organic precursor synthesized from the amide of the DPA (2,6-pyridinedicarboxylic acid) with APTES (aminopropyltriethoxysilane) in the presence or absence of the non-ionic surfactant F-127. The emission spectrum of the luminescent Eu(III) complex obtained was used to sense and compare the environment of the lanthanide in the amorphous matrices as well as the accessibility of the material by means of the quenching of its luminescence by Cu(II). Solid devices were built to test and compare their performances as potential sensors of Cu(II) in terms of the values of the Stern–Volmer constants in the quenching experiments. Templated materials with F127 showed the best response ($K_{SV} = 1.2 \; 10^5 \; M^{-1}$) when compared with the results obtained for the non-templated ones at different synthesis conditions permitting the *in situ* detection of Cu(II) in solution down to the 0.05 ppm level.

Introduction

The use of bridged silsesquioxanes $[(RO)_3Si]_n$-R′ ($n \geq 2$) as precursors to include an organic functional group inside the channel walls of a mesoporous matrix gave rise to novel hybrid materials known as PMOs (periodic mesoporous organosilicas).[1–3] The functionalisation of these frameworks to include chromophores[4] with suitable optical properties has been the subject of many studies, with particular interest in those related with lanthanide-ion based matrices.[5–7]

Lanthanide ions display a well-defined luminescence characterized by narrow and highly structured emission bands with lifetimes in the millisecond timescale.[8–11] The excited state long lifetime is not quenched by O_2. For luminescence quenching-based sensors, this is a great advantage compared to phosphorescence quenching of organic compounds because it makes the detection possible in non-degassed media. Lanthanide complexes are valuable alternative probes to conventional dyes because the emission is observed in the green–red region of the spectrum, where few compounds in natural waters and biological systems emit light.

Lanthanides have low absorption coefficients but this drawback can be overcome by including in the coordination sphere of the metal an organic chromophore with a large absorption cross section and with suitable energy transfer characteristics to populate the ion-centered emitting states.[12–15]

The sharp and intense emission bands of Eu(III) complexes are also used as a probe to sense the chemical environment in glass films and gels[16–19] in which X-ray diffraction techniques cannot reveal the structure of the system.

Undoubtedly, the lanthanides' luminescent properties make these compounds especially profitable for the design of luminescent labels[20–23] and sensors.[24–26] Luminescence detection of fiber optic coated sensing layers is a very adequate approach for low perturbation and fast measurement of analytes.[27–31]

One of the matrices that has been most studied due to their good thermal and mechanical properties is the silica network.[32,33] Hybrid materials obtained by the hydrolysis and condensation of organoalkylsilanes from a sol–gel technique, have been widely used to immobilize organic or inorganic molecules[34–36] in a porous glass or film[37] at low temperature. In particular, Eu(III) complexes and chelates have also been incorporated into these hybrid silica matrices to build optical sensors of pH,[38] anions[26] and cations.[39,40]

Transition metal ions are known to be efficient quenchers of the emission of lanthanide complexes. Cu(II) ions act much more efficiently than any other fourth period transition metal cations.[41–43] Electronic energy transfer is the quenching mechanism postulated to operate in these cases.[21,23,43–45]

In this work we use the sol–gel technique to synthesize luminescent Eu(III) porous materials from a bis(trialkoxysilyl) organic precursor synthesised from the diamide of DPA (2,6-pyridinedicarboxylic acid) with APTES (aminopropyltriethoxysilane) in the presence or absence of a non-ionic surfactant F-127 ($EO_{97}PO_{69}EO_{97}$, where EO represents the ethylene oxide and PO represents the propylene oxide) and tetraethylortosilicate (TEOS) as crosslinker. The luminescent amorphous materials obtained were characterized by powder X-ray diffraction (XRD), infrared absorption and luminescence emission spectroscopy in the UV-visible. The lifetimes of Eu(III) complex were also measured to evaluate the number of water molecules coordinated to the lanthanide in the matrices.[46] The ratio of the emission bands $^7F_2 : {}^7F_1$ of the emission spectra of Eu(III) were compared for the different materials to evaluate the environment of the ion in the matrix.[19] The accessibility of the Eu(III) centers in the materials was tested *via* the deactivation of the luminescence of the lanthanide ion by Cu(II) in aqueous solution. Thin films of the prepared gels were built to test and compare their performance as potential sensors of Cu(II) in terms of the values of their Stern–Volmer constant in the quenching experiments. The most adequate matrix permits the *in situ* detection of Cu(II) down to the 0.05 ppm level.

INQUIMAE and Departamento de Química Inorgánica, Analítica y Química Física, Facultad de Ciencias Exactas y Naturales, Universidad de Buenos Aires, Pabellón 2, Ciudad Universitaria, C1428EHA Buenos Aires, Argentina. E-mail: barja@qi.fcen.uba.ar, pedro@qi.fcen.uba.ar; Fax: +54 (0)11 4576 3341
† Electronic supplementary information (ESI) available: Typical micrograph of particles of matrix **M**. See DOI: 10.1039/b806071a

Experimental

Chemicals

Copper (II) chloride-dihydrate and pyridine were obtained from Mallinckrodt, $Eu(NO_3)_3 \cdot 6H_2O$ 99%, was obtained from Fluka Chemie AG. They were used as received. Ethyl ether, from Sigma, was dried under Na and immediately used. DPA (2,6-pyridinedicarboxylic) acid and APTES (3-aminopropyltriethoxysilane), TEOS, TMOS and PVAc were all from Aldrich. Water was from a Milli-Q system. F127 was obtained from Fluka (FW 13800). $Na_3Eu(DPA)_3 \cdot 15H_2O$ was synthesised according to literature methods.[47] Cl_2SO_2 (previously distilled) and methylene chloride (used as received) were from Merck. HCl (c) and NH_3(c) were from Mallinckrodt.

X-Ray diffraction measurements

The samples were analyzed by powder XRD with a Siemens D-5000 Difractometer. Cu Kα radiation ($\lambda = 1.542$ Å) was used in the analysis.

Steady state absorption and emission spectra and quenching measurements

IR spectra were obtained in KBr pellets with a Nicolet 8700 FTIR equipment. The steady state emission spectra of all the compounds were recorded on a PTI QuantaMaster QM-1 luminescence spectrometer. Samples were placed in a 1 cm square quartz fluorescence cuvette and measured in right angle geometry. Excitation wavelength was 290 nm. For quenching experiments, the emission wavelength was 615 nm. Excitation and emission bandwidths were set to 8 and 4 nm, respectively. The experimental points plotted in the graphs of the quenching experiments were obtained from the emission intensity averaged over a period of 10 minutes. These average values are affected by an error not higher than 3%.

The linear regression coefficients of the linear fits (r^2) of normal or modified Stern–Volmer graphs were 0.9989, 0.9958, 0.9909 and 0.9989 for matrices **A**, **B**, **C** and **M**, respectively.

Luminescence lifetimes. To measure the lanthanide centered emission, samples were excited with the second harmonics of a Nd:YAG laser (Spectron), which delivered pulses of 8 ns FWHM at 10 Hz at 354 nm. Emitted light was collected by an optical fiber in front face geometry, passed through a monochromator, and was detected at 615 nm with 8 nm bandwidth. Light was measured with a R928 Hamamatsu photomultiplier and the transient signal was processed by a HP54502 digital oscilloscope and stored in a PC. The traces were fitted to a single exponential decay. The goodness of the fit was judged by a homogeneous time-distribution of residuals.

Synthesis of the compounds

Synthesis of the hybrid DPA silanised precursor (HSP). (3.0 mmol) of DPA were dissolved in excess Cl_2SO_2 and refluxed for 8 hours under N_2. 0.6 g (2.94 mmol) of the white solid 2,6-pyridinedicarbonyl dichloride obtained was filtered and dissolved in 50 mL of dry diethyl ether. 0.65 g (5.4 mmol) of APTES and 0.5 mL of pyridine (0.49 g, 6.2 mmol) were dissolved in 20 mL of dry diethyl ether and this solution was added dropwise to the DPA diethyl ether solution always under N_2 and left stirring for 4 hours. The white pyridinium chloride was filtered and the diethyl ether and pyridine, evaporated. The transparent light-yellow oil obtained corresponds to the DPA silanised ligand as corroborated by ^{1}H NMR and IR spectra. Its molecular mass is 573 g mol^{-1}.[48]

Synthesis of an Eu(III)–HSP matrix (A). 0.578 g (1 mmol) of HSP obtained from the previous step was dissolved in 600 μL of anhydrous ethanol under stirring until a transparent gel was obtained. 75 mg (0.17 mmol) of $Eu(NO_3)_3 \cdot 6H_2O$ dissolved in approximately 600 μL of anhydrous ethanol were added to the transparent HSP gel and the slightly pink final mixture was left under stirring for 45 minutes. 18 μL of H_2O and 5 μL of HCl (c) were also added to reach a final pH = 2, under stirring. The final mixture was left without stirring in a sealed flask and gellified in 24 h, the white powder obtained was dried under vacuum at 45 °C for 3 days. The molar ratio in HSP : H_2O : Eu(III) is 1 : 2.3 : 0.17 (see Scheme 1).
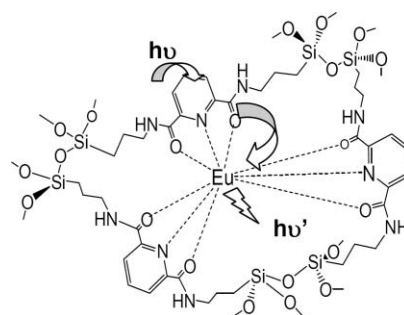
Scheme 1 Proposed structure for matrix **A** showing the antennae mechanism for the emission of Eu(III).

Synthesis of a Eu(III)–HSP–TEOS matrix in acid media (B). 0.6609 g (3.17 mmol) of TEOS and 0.180 g (0.314 mmol) of HSP were dissolved in 500 μL of ethanol under stirring until a transparent gel was formed. Separately, 26.5 mg of $Eu(NO_3)_3 \cdot 6H_2O$ (6×10^{-2} mmol) were dissolved in 90 μL of acidified water (HCl, pH = 2–2.5) with 300 μL of ethanol. The $Eu(NO_3)_3 \cdot 6H_2O$ solution was added to the HSP–TEOS mixture and left under stirring for 12 hours. After 5 days, the transparent gel obtained turned into a white powder after drying in vacuum at 40 °C. The molar ratio for this synthesis was: 1 : 10 : 17 : 0.2 in HSP : TEOS : H_2O : Eu(III)

Synthesis of a Eu(III)–HSP–TMOS matrix in ammonia (C). 0.2686 g (1.8 mmol) of TMOS and 0.103 g (0.18 mmol) of HSP were mixed with 30 μL of an aqueous solution of ammonia (pH = 9.5–10) and 600 μL of anhydrous ethanol. The pH was adjusted with microlitres of NH_3 (35% w/w density 0.88 g mL^{-1}).

Separately, 0.0230 g (0.052 mmol) of $Eu(NO_3)_3 \cdot 6H_2O$ were dissolved in 130 μL of an aqueous solution of ammonia (pH = 9.5–10) and 600 μL of anhydrous ethanol. The pH was adjusted with microlitres of NH_3(c). The Eu(III) solution was added to the HSP–TMOS gel while stirring, a white solid particulate gel was formed almost immediately after mixing. The powder was dried in vacuum at 40 °C for 24 h.

The molar ratio for this synthesis was: 1 : 10 : 9.2 : 0.3 in HSP : TMOS : H_2O : Eu(III)

Synthesis of a mesoporous hybrid Eu(III)–HSP–TEOS silica matrix (M). 0.1598 g (0.0013 mmol) of F127 and 2.0526 g (9.85 mmol) of TEOS were mixed and dissolved with 0.8392 g of an aqueous solution of HCl (pH = 1.5). After 40 minutes of stirring, the dissolution was complete. Then, 0.1015 g (0.18 mmol) of HSP was added to the mixture with 43 mg of $Eu(NO_3)_3 \cdot 6H_2O$ (9.6.10^{-2} mmol) and stirred until a clear transparent mixture was obtained. The molar ratio in the synthesis was: 1 : 55 : 255 : 0.07 : 0.5 in HSP : TEOS : H_2O : F127 : Eu(III). The excess ethanol was slowly extracted under vacuum until the mixture became viscous. The gel formed was left at room temperature in a sealed flask for 4 days. The transparent monolith obtained was hydrothermally treated at 100 °C for 24 h for better structuration. The surfactant was removed by a hot Soxhlet extraction with acidified ethanol (0.1 M in HCl) for 3 days and was finally washed with ethanol. A light-yellow powder was obtained.

Preparation of a sensor layer. 500 μL of a solution of 4 g of PVAc per 100 mL of Cl_2CH_2 were added to 20–25 mg of grounded luminescent powder (**A**, **B**, **C** or **M** separately) and stirred vigorously for 30 min (particle size 1–10 μm).† Portions of this suspension (50 μL) were placed on a microscope glass slide (9 × 20 mm) and left drying first at room temperature and then at 50 °C for approximately 2 hours. Once the sample was dry, a white spot was obtained on the glass. This spot (approximately 10 μm thick) contains the luminescent Eu(III) hybrid matrix (**A**, **B**, **C** or **M**) immersed in the PVAc supporting polymer. The white spot kept firmly attached to the surface of the glass support and was used as the (hereafter-called) sensor. Except when indicated, all layers were allowed to equilibrate with distilled water overnight prior to measurements.

Luminescence measurements with the sensors. The sensors were fixed firmly to a diagonal slit carved in the inside of a Teflon cap of a 1 cm square quartz fluorescence cuvette in such a way that the sensor was placed in a front face geometry inside the cuvette containing the test Cu(II) aqueous solution. The luminescent response was measured in situ. The sensors were always immersed in the solutions and kept in the spectrofluorimeter in the same position. A 2 mm diameter hole in the cap enables the addition and replacement of the quencher solution while keeping the cuvette in place. The samples were always stirred during the experiments.

The sensor was allowed to equilibrate with water to record the zero quencher intensity (I_o, no metal added). Afterwards, aliquots of a Cu(II) solution were added to the cuvette with the sensor in place by means of a microsyringe while stirring. The steady state emission of each solution was measured after 500 s under stirring.

Results

X-Ray diffraction measurements

The powder X-ray diffraction (XRD) patterns in the range of 0 to 60° (2θ) were measured for the four matrices **A**, **B**, **C** and **M** (See Fig. 1). All the samples are amorphous with two broad bands with maxima at $2\theta_1 \approx 10°$ (Matrices **A**, **B** and **C**) and $2\theta_2 \approx 23°$ (Matrices **A**, **B**, **C** and **M**). Table 1 shows the $2\theta_1$ and $2\theta_2$ values together with their corresponding Bragg spacing, d_1 and d_2.
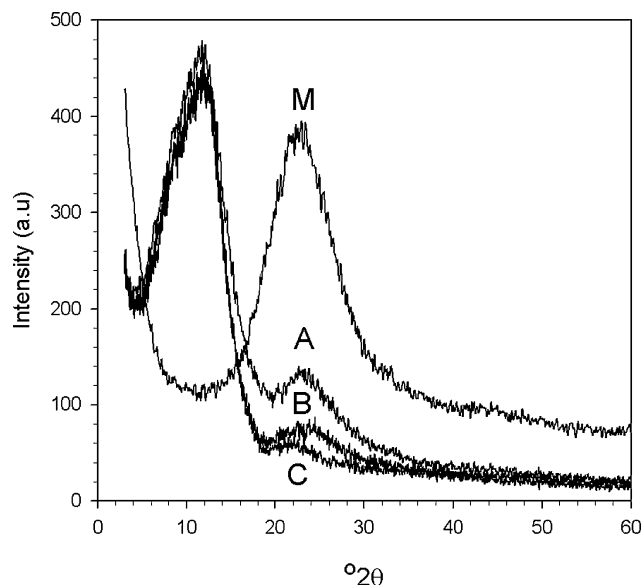
Fig. 1 X-Ray diffraction patterns in the range of $5° < (2\theta) < 60°$ for matrices **A**, **B**, **C** and **M**.

The diffraction band at the larger angle $2\theta_2 \approx 23°$ is present in all the samples, and can be associated with the shorter structural distances (≈ 4 Å). This $2\theta_2$ value is similar to that obtained for fused silica ($2\theta = 21.16°$) and for silica xerogels obtained from 100% TMOS ($2\theta = 22.9°$).[49] The diffraction band at the lower angle $2\theta_2 \approx 10°$ is present in all the samples except in matrix **M**, where the ratio HSP–siloxane is the lowest (0.018, compared with 0.1 of matrices **B** and **C**). From the powder X-ray patterns of ormosils of TMOS–MTMOS, a value of $2\theta_1 = 7$–$10°$ was reported[49] which was associated with the spacing between silicon atoms attached to the organic methyl groups.

From Fig. 1 it is clear that the band at $2\theta_1 \approx 10°$ dominates the diffractogram for matrices **A**, **B** and **C**. For matrix **A** (100% HSP) the band at $2\theta_1 \approx 10°$ is 21 times more intense than the band at $2\theta_2 \approx 23°$, having this later band a very low intensity. For **B** and **C** matrices, where the HSP–TEOS mole ratio is 1 : 10, the $2\theta_2/2\theta_1$ relative intensities lower to 6.5 and 9, respectively.

Table 1 Experimental synthesis ratios of reactants and XRD results for matrices **A**, **B**, **C** and **M**

Matrix	Precursors	HSP	TEOS	H_2O	Eu(III)	F127	$2\theta_1$/deg	d_1/Å	$2\theta_2$/deg	d_2/Å
Matrix **A**	HSP	1	—	2.3	0.17	—	10.2	8.67	22	4.04
Matrix **B**	HSP/TEOS/H^+	1	10	17	0.2	—	10.6	8.35	23.2	3.83
Matrix **C**	HSP/TEOS/OH^-	1	10	9.2	0.3	—	10.5	8.43	23	3.87
Matrix **M**	HSP/TEOS/F127/H^+	1	55	255	0.5	0.07	—	—	23	3.87

According to these results, we associate the bands at $2\theta_1 \approx 10°$ ($d_1 = 8.7$ Å) with the spacing between silicon atoms bound to the organic precursor HSP, and the band at $2\theta_2 \approx 23°$ ($d_2 = 4$ Å) with the spacing between silicon atoms located in the inorganic network. Similar broad reflections were obtained for polimethylsesquioxanes ($d_1 = 8.7$ Å and $d_2 = 3.6$ Å) synthesized from preaminolysis of methyltrichlorosilane.[2] Matrix **M** has only one broad band at $2\theta_2 \approx 23°$ which would correspond to the spacing of silicon atoms of an inorganic silica network. The lack of the second band at $2\theta_1 \approx 10°$ could be interpreted in terms of the high dilution of the organic precursor (HSP–TEOS = 1 : 55) in the matrix.

Infrared spectroscopy

Fig. 2 shows the infrared transmission spectra of the powders of matrices **A**, **B**, **C** and **M**. The assignment of the main bands of these matrices, and of the free HSP are shown in Table 2.
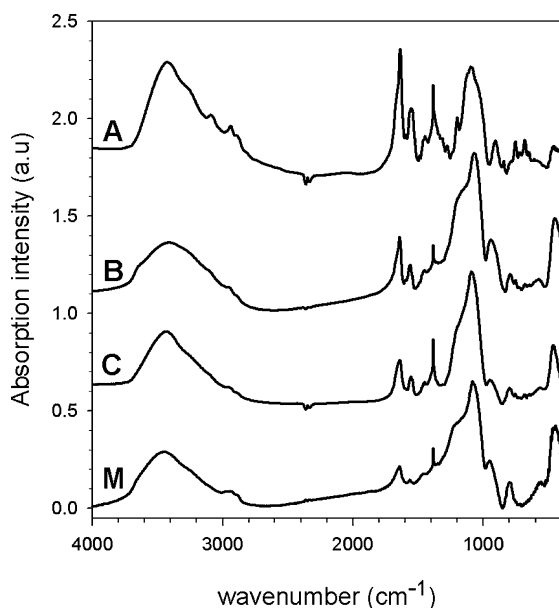
Fig. 2 Infrared spectra of matrices **A**, **B**, **C** and **M** in KBr pellets. Spectra A, B and C are shifted in the vertical axes.

The $\nu_{C=O}$ vibration is located at 1653 cm⁻¹ in the free HSP and at 1637, 1642, 1637 and 1634 cm⁻¹ for matrices **A**, **B**, **C** and **M**, respectively. In all cases, a $\Delta\nu_{C=O} \approx 15$–20 cm⁻¹ to lower wavelengths is observed which can be attributed to the formation of the Eu(III) complex in the bulk of the matrix thus lowering the electronic density of the C=O bond due to the coordination with the lanthanide.

In aromatic amide complexes of Eu(III) ν_{CO} in the range 1610–1651 cm⁻¹ are reported.[50,51] These values fall within the range reported in Table 2 for matrix A ($\nu_{CO} = 1637$ cm⁻¹), matrix B ($\nu_{CO} = 1642$ cm⁻¹), matrix C ($\nu_{CO} = 1641$ cm⁻¹) and matrix M ($\nu_{CO} = 1634$ cm⁻¹).

The broad absorption band located in the range 1000–1200 cm⁻¹ can be assigned to the stretching of the Si–O–Si arising from the hydrolysis and condensation reaction of HSP (matrix **A**) or from the hydrolysis and condensation reactions of HSP–TEOS in matrices **B**, **C** and **M**. The intensity ratio $\nu_{C=O}/\nu_{SiOSi}$ is inversely proportional to the amount of crosslinker TEOS present in the synthesis of the gel. This ratio is the highest for matrix **A** where no TEOS was added and is the lowest for matrix **M** where the HSP–TEOS ratio falls to 1 : 50.

The nature of a shoulder observed at $\approx$1250 cm⁻¹, resulting from a longitudinal mode of the Si–O–Si stretching, has been attributed to long range coupling of coulombic interactions in silica sol–gel materials[52] and its intensity is enhanced at larger porosities not only in powders but also in thin films.[53] From Fig. 2, the spectrum of matrix **A** shows no broad shoulder at 1200–1250 cm⁻¹ (a band at 1196 cm⁻¹ is also present in the HSP precursor) indicating the non-porosity of the material. The rest of the matrices show shoulders at $\approx$1200 cm⁻¹ but only in matrix **M** the value is shifted to 1230 cm⁻¹.

The bands associated with the Si–O–C, Si–C are overlapped with the strong absorption bands of the Si–O–Si vibration modes in the 1200–1000 cm⁻¹ range.

Emission properties of the Eu(III)-silica matrices and environment of the Eu(III) sites

The normalized emission spectra of matrices **A**, **B**, **C** and **M** show the characteristic Eu(III) centered transition bands ($^5D_0 \rightarrow {}^7F_J$) for $J = 0, 1, 2, 3$ and 4 at *ca.* 578, 590, 615, 650 and 698 nm, respectively. Due to their similar spectral profiles only two of them are shown in Fig. 3. In all matrices, the ratio of the intensities for the ($^5D_0 \rightarrow {}^7F_2$) to that of the ($^5D_0 \rightarrow {}^7F_1$) (hereafter called I_{F2}/I_{F1}) is much higher than 1, as observed in amorphous silica materials.[19] The higher this ratio, the lower is the symmetry of the local environment of the Eu(III) ions in the matrix.[16–18] The values for the intensity ratio ($I_{F2} : I_{F1}$) were measured for all the matrices obtaining: 5.6, 4.9, 5.4 and 4.8 for matrices **A**, **B**, **C** and **M**, respectively (see Table 3). These values are, as expected, all higher than the value

Table 2 IR band assignments for the matrices **A**, **B**, **C** and **M** in KBr pellets

Band assignment	Free HSP ν/cm^{-1}	Matrix A ν/cm^{-1}	Matrix B ν/cm^{-1}	Matrix C ν/cm^{-1}	Matrix M ν/cm^{-1}
ν OH	3500	3424	3449	3434	3447
ν CO	1653	1637	1642	1641	1634
δ NH–ν CN	1539	1554	1560	1554	1559
δ CH₃	1386	1384	1384	1384	1384
ν_{ass} Si–O–Si	—	1196, 1100	1070, 1200 (sh)	1090, 1200 (sh)	1079, 1230 (sh)
ν Si–OH		906	942	951	951
ν_{ass} Si–O–Si	789	753, 681	793	799	796
ρ Si–O–Si	—	446	444	463	444

Table 3 Emission intensity ratio ($I_{F2} : I_{F1}$ see text[a]), experimental lifetimes (τ_{exp}), calculated radiative (k_r) and nonradiative (k_{nr}) $^5D_0$ decay rate constants and number of water molecules (n_w) coordinated to the Eu(III) ions in matrices **A**, **B**, **C** and **M**, (see eqn (1)–(3) in the text)

Matrix	Precursors	$I_{F2} : I_{F1}$	τ_{exp}/ms	k_r/ms^{-1}	k_{nr}/ms^{-1}	n_w
Matrix **A**	HSP	5.6	0.66	0.23	0.78	1.4
Matrix **B**	HSP/TEOS/H$^+$	4.9	0.57	0.22	0.65	1.6
Matrix **C**	HSP/TEOS/OH$^-$	5.4	0.30	0.26	0.33	3.2
Matrix **M**	HSP/TEOS/F127/H$^+$	4.8	0.29	0.22	0.31	3.4

[a] See section on Emission properties of the Eu(III)-silica matrices and environment of the Eu(III) sites.
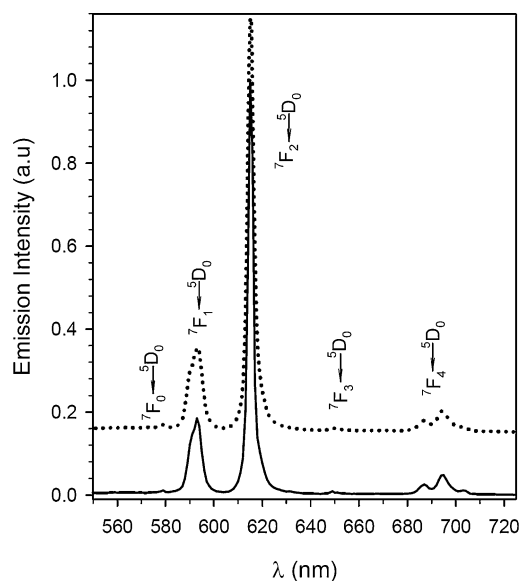
Fig. 3 Normalized emission spectra of matrix **A** (dotted line) shifted upwards for clarity, and matrix **B** (solid line), at room temperature. The characteristic Eu(III) centered emission $^5D_0 \rightarrow {}^7F_J$ bands are also indicated. (λ_{exc}= 290 nm).

obtained in the emission spectrum of the pure solid Na$_3$Eu(DPA)$_3$ complex ($I_{F2} : I_{F1} = 3.2$) but are comparable to the one obtained in the emission spectrum of the Na$_3$Eu(DPA)$_3$ complex physically entrapped in an inorganic silica matrix ($I_{F2} : I_{F1} = 5.3$). This is an evidence that the Eu(III) ions sense a similar DPA environment when they are simply occluded in an inorganic silica matrix as the Na$_3$Eu(DPA)$_3$ complex or when they are added during the synthesis to finally form the hybrid silica–DPA matrix. In both cases the site symmetry of the Eu(III) center lowers from the pure solid complex to an C_s or even lower point-group symmetry in glasses.[16] Table 3 also shows the emission lifetimes for the Eu(III)–$^5D_0$ excited state in the four matrices obtained from their emission decays at 615 nm at room temperature. The values of the lifetimes for the four matrices **A**, **B**, **C** and **M** (0.7–0.3 ms) are all shorter when compared with the lifetime of Eu(III) in the solid Na$_3$Eu(DPA)$_3$ complex (1.3 ms).[54]

The values of the excited state lifetimes of the matrices suggest that part of the Eu(III) ions would retain OH$^-$ groups from the alkoxides or water molecules in their first coordination sphere causing the decrease in the excited state lifetimes of the lanthanide. It is known that slight differences in the water content give rise to important changes in the lifetimes of the Eu(III) ion.[46]

The mean number of water molecules, n_w, coordinated to the Eu(III) ion in the matrices can be calculated from the experimental lifetimes ($k_{exp} = 1/\tau_{exp}$) of the excited states as suggested by Horrocks.[54]

$$n_W = 1.05(k_{exp} - k_r) \qquad (1)$$

$$k_{exp} = k_r + k_{nr} \qquad (2)$$

where k_r and k_{nr} are the radiative and non radiative decay rate constants, respectively, expressed in units of ms^{-1}.

The radiative contribution k_r can be calculated from the relative intensities of the Eu(III) centered transition bands[55,56] ($^5D_0 \rightarrow {}^7F_J$) for $J = 0$–4.

$$k_r = (A_{0-1} \cdot E_{0-1} / S_{0-1}) \cdot \sum (S_{0-J} / E_{0-J}) \qquad (3)$$

where A_{0-1} is the Einstein's coefficient of spontaneous emission for the $^5D_0 \rightarrow {}^7F_1$ (in general considered as 50 s^{-1}), and S_{0-J} and E_{0-J} are the integrated intensity and the energy of the $^5D_0 \rightarrow {}^7F_J$ transition, respectively.

The quantum efficiency of emission from the lanthanide center can be calculated as: $\phi_{em} = k_r/k_{exp}$. This gives values of 0.15, 0.13, 0.08 and 0.06 for matrices **A**, **B**, **C** and **M**, respectively.

Table 3 shows the summary of k_r, k_{nr} and the number of water molecules (n_w) coordinated to the Eu(III) center in matrices **A**, **B**, **C** and **M**, calculated with the eqn (1)–(3). These results show that matrix **A** and matrix **B** contain only one or two water molecules in the first coordination sphere of the Eu(III) ion, while matrices C and M contain both 3 water molecules. This difference in the water content is responsible for the shorter lifetimes of Eu(III) in matrices **C** and **M**.

The intensity of the spectra when excited at 290 nm (absorption maximum of the DPA ligand) are more than one order of magnitude higher than the intensity of the spectra when excited at 394 nm (absorption band of the Eu(III) ion), indicating that the DPA moiety of the HSP precursor efficiently coordinates the sites of the first coordination sphere of the Eu(III), and that the antenna effect is conserved.

Quenching experiments in aqueous solution

The Stern–Volmer equation has been widely used to evaluate the relationship between the relative fluorescence intensity of an immobilized luminescent probe and the measured analyte concentration. Coated fiber sensors, enzyme-mediated sensors or gas sensors are some examples.[27]

Fig. 4 shows the steady state Stern–Volmer plot for the deactivation of the emission of thin layers of matrices **A** and **B** by Cu(II) in aqueous solution. The Stern–Volmer constants obtained from their slopes are $K_{SV} = 2 \times 10^2$ M^{-1}, equal for matrices **A** and **B**, within experimental uncertainty.
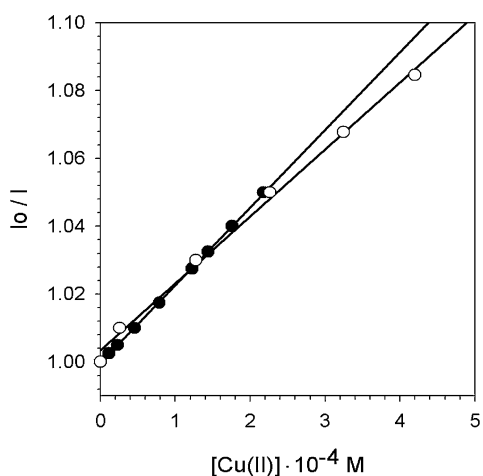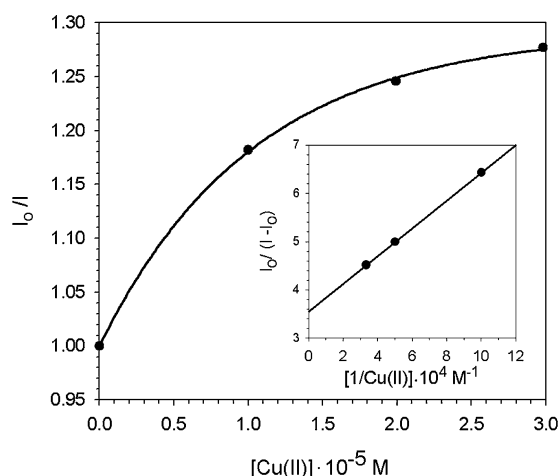
Fig. 4 Stern–Volmer plots for the deactivation of sensors of matrices **A** (black circles) and **B** (white circles) by Cu(II) in aqueous solution. The excitation and emission wavelengths are 290 and 615 nm, respectively.

Contrary to the linear dependence observed for matrices **A** and **B**, the quenching plots of sensors of matrices **C** and **M** show a downward curvature in their correspondent Stern–Volmer graphs (Fig. 5 and 6, respectively). These non-linear dependence can be rationalized in terms of the existence of two different types of Eu(III) emitting centers in the sensor:[57] a quenchable one characterized by its Stern–Volmer constant K_{SV}; and an unquenchable population whose luminescence is independent of the quencher concentration. These two populations can be analyzed using a modified form of the Stern–Volmer equation. The two-state model represented by the modified Stern–Volmer eqn (4)

$$\frac{I_o}{\Delta I} = \frac{1}{f_a} + \frac{1}{f_a \cdot K_{SV}} \cdot \frac{1}{\left[Cu^{2+} \right]} \qquad (4)$$
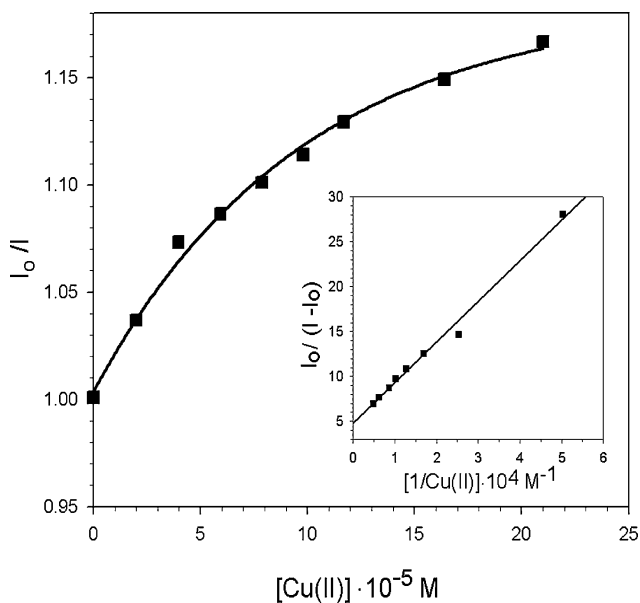
Fig. 5 Stern–Volmer plot and modified Stern–Volmer plot (inset) for the deactivation of a sensor of matrix **C** by Cu(II) in aqueous solution. The excitation and emission wavelengths are 290 and 615 nm, respectively.

Fig. 6 Stern–Volmer plot and modified Stern–Volmer plot (inset) for the deactivation of a sensor of matrix **M** by Cu(II) in aqueous solution. The excitation and emission wavelengths are 290 and 615 nm, respectively.

is the simplest one to describe an heterogeneous system. A plot of $I_o/\Delta I$ against $1/[Cu(II)]$ where $\Delta I = I_o - I$, I_o and I being the emission intensity in the absence of added Cu(II) and in the presence of added Cu(II) in solution, respectively, yields from the intercept, the fraction of quenchable sites, f_a, and the Stern–Volmer constant from the slope, $(f_a \cdot K_{SV})^{-1}$. The representation of this linear modified Stern–Volmer equation for the deactivation of sensors of matrices **C** and **M** by Cu(II) in solution are shown in the insets of Fig. 5 and 6, respectively. The corresponding K_{SV} and f_a values are: $K_{SV} = 9.6 \times 10^3$ M^{-1}, $f_a = 0.21$ for sensor of matrix **C** and $K_{SV} = 1.2 \times 10^5$ M^{-1}, $f_a = 0.28$ for a sensor of matrix **M**.

The lifetimes of the Eu(III) center were measured in aqueous solution for the sensor layer prepared with matrix **M**. It was observed that the addition of quencher Cu(II) did not modify the value of the lifetime of the Eu(III) ion in the sensor layer in pure water. This result indicates that the deactivation of the Eu(III) ion in the sensor by Cu(II) is not a dynamic process, contrary to what was previously measured in aqueous solution in which the simultaneous dynamic and static deactivation was observed.[58]

As expected for a class II materials, the Eu(III) complex never leached from the solid matrices of the sensor to the aqueous solution even after several hours of immersion.

Discussion

Emission sensitization and emission spectra show that Eu(III) is efficiently coordinated by DPA centers in all the matrices.

Thin layers of matrices **A** and **B** can detect approximately 30 ppm of Cu(II) in solution for a 10% emission deactivation of the Eu(III) emission center. On the other hand, layers prepared with matrices **C** and **M** are able to detect 0.66 and 0.05 ppm of Cu(II) in solution, respectively.

The linearization of the Stern–Volmer plots obtained for the quenching experiments of the layers from matrices **C** and **M** indicates that not all the Eu(III) sites of the sensor matrix are equally exposed to the metal ions. Only the fraction of accessible complexes (*ca.* 1/4 for matrix M and 1/5 for matrix **C**) is the responsible for the quenching of the Eu(III) centers of the sensors. The remaining active centers are buried enough in the matrix of the

sensors and do not experience any luminescence deactivation even after long periods of hydration. The simplest heterogeneous model for quenching, that we used in this work, involving only two types of sensing sites, ones that can be quenched and ones that cannot be quenched at all, gives a satisfactory description of the quenching process. In the context of a more general microheterogeneous model with a distribution of quenching sites, that is physically meaningful to describe the system,[59,60] one can interpret that this distribution is well represented by a bimodal one of quenchable and non quenchable sites.

The difference in two or more orders of magnitude in the values of the Stern–Volmer constants K_{SV} of the sensors must rely on the difference in the preparation of their matrices and on their different porosities.

The sensor of matrix **M** gives the lowest detection limit for Cu(II) (0.05 ppm of Cu(II) for a 10% of deactivation, $K_{SV} = 1.2 \times 10^5$ M^{-1}), which can be related with the high porosity obtained by the inclusion of a surfactant in the matrix. The presence of a shoulder at 1230 cm^{-1} in matrix **M** also supports these results as discussed in the IR section.

As shown in Table 3, the water content for the matrices is different. Matrices **C** and **M** contain twice the number of water molecules in the first coordination sphere of the Eu(III) ion than matrices **A** and **B**. A possible explanation for these differences can be directly related with the Eu : HSP molar ratio used in the synthesis of each matrix.

Matrices **A** and **B** have more than three HSP molecules per Eu(III) ion (Eu : HSP = 1 : 6 and 1 : 5 for matrices **A** and **B**, respectively), matrix **C** is near to the stoichiometric ratio (Eu : HSP = 1 : 3) and matrix **M** has an excess of Eu(III) content (Eu : HSP = 1 : 2) when compared with the stoichiometric ratio. Thus, in matrices **A** and **B**, the average number of water molecules is the lowest (see Table 3, $n_w = 1$–1.5) in accordance with an almost fully coordinated Eu(III) sphere by the HSP ligands.

For matrices **C** and **M**, the number of water molecules is around 3 (see Table 1) pointing out that, in average, only six out of the nine sites of the coordination sphere of the Eu(III) are coordinated to the HSP ligand (three sites per HSP).

In view of these results, the Eu(III) center has HSP-free sites that can be reached out by the Cu(II) quencher ions to replace the water molecules and provoke the deactivation of the Eu(III) luminescence. The fact that the lifetime of the excited state of the lanthanide in matrix **M** does not change with added Cu(II) is a direct proof that the deactivation is carried out mainly through a static process. Moreover, it is known that Cu(II) forms 1 : 1 and 1 : 2 complexes with DPA as ligand with $K_1 = 1.4.10^9$ M^{-1} and $K_2 = 2.4.10^7$ M^{-1} in water.[61] From these values and from those for the complexes of Eu(III) with DPA ($K_1 = 7.10^8$ M^{-1}, $K_2 = 1.4.10^7$ M^{-1} and $K_3 = 3.2.10^5$ M^{-1} also in water)[61] it can be inferred that a ligand exchange given by the eqn (5) is favored with a $K_{eq} = 100$.

$$[Eu(DPA)_2]^- + Cu^{2+} \rightarrow [Eu(DPA)]^+ + [Cu(DPA)] \quad (5)$$

Eu(III) localized in environments with three water molecules are more labile to move and be displaced from the DPA coordination by Cu(II) than the Eu(III) ions coordinated in a three DPA environment with their ligands bound to the organosilicon network. A displacement of one ligand to accommodate Cu(II) would require a major matrix rearrangement. Regarding the higher affinity of Cu(II) for DPA than Eu(III) this could explain the higher static quenching observed.

In the labile sites, the Eu(III) complexation by the DPA centers must be reverted upon Cu(II) removal considering that there is no Eu(III) leaching from these matrices.

The sites termed as non-quenchable in the **C** and **M** matrices might well have K_{SV} in the order of 10^2 M^{-1}, typical values of matrices **A** and **B**, which can are negligible when compared to as 10^4–10^5 M^{-1} values of the accessible sites.

Matrices **A** and **B** seem not to be porous enough to detect Cu(II) at a sub-ppm level.

It is known that systems prepared from base-catalyzed media display a larger pore mean size when compared with acid catalyzed ones.[32] This fact seems to apply also to hybrid materials in view of the good performance of the sensor prepared from the ammonia synthesized matrix **C** in the quenching experiments when compared with the acid catalyzed sensors **A** and **B**. The low accessibility of the sensors of matrices **A** and **B** to the Eu(III) centers could be associated with a more stiff hybrid network, specially for matrix **A** where no crosslinker TEOS was added.

The value 1.2×10^5 M^{-1} for the Stern–Volmer constant of the sensor of matrix **M** is very close to what was measured in aqueous solution for the quenching of $Eu[(DPA)_3]^{3-}$ by Cu(II) : 3.7×10^5 M^{-1}.[58]

In other words, the deactivation of the emission of a luminescent center in a solid matrix is an interesting way to get an insight to the true accessibility of the material in solution. In fact, the accessibility of the diamine groups of several amine-functionalized periodic mesoporous organosilicas (PMOs) has already been estimated by Burleigh et al.[62] through the adsorption of Cu(II) in aqueous solutions. In that work, the change in the Cu(II) concentration before and after the immersion in the hybrid matrix was measured spectrophotometrically at the maximum of absorption of the 1 : 1 diamine complex formed between the amino groups of the hybrid matrix and the Cu(II) ions. Walcarius et al. also examined the influence of the structure of five mesostructured silicas, grafted with amino and thiol groups by means of the access of H$^+$, Hg(II) and Cu(II) to the binding sites.[63]

The layers, obtained using bridged silsesquioxanes as precursors to include an organic functional group inside the channel walls of a matrix, showed an excellent performance in terms of sensibility and low detection limits for the in situ detection of ions in aqueous solution when compared with the physically entrapped Na$_3$Eu(DPA)$_3$ in an inorganic sol–gel matrix.[64] It is worth mentioning that good optical quality of the sol–gel matrices is not necessary to build up the sensors: transparency is a non-trivial feature to achieve when dealing with hybrid materials. As expected for a covalently-bound active fluorophore, no leaching of the sensing material Eu(III) from the matrix is observed even after long periods of exposure to the aqueous solution, an essential feature in favor of the long term utility of a sensor device.

Abbreviations

DPA: 2,6-pyridinedicarboxylic acid; TMOS: tetramethoxysilane; PVAc: polyvinyl acetate.

References

1 C. Yoshina-Ishii, T. Asefa, N. Coombs, J. MacLachlan and A. Ozin, Periodic mesoporous organosilicas, PMOs: fusion of organic and inorganic chemistry inside the channel walls of hexagonal mesoporous silica, *Chem. Commun.*, 1999, 2539–2540.

2 R. H. Baney, M. Itoh, A. Sakakibara and T. Suzuki, Silsesquioxanes, *Chem. Rev.*, 1995, **95**, 1409–1430.

3 B. J. Melde, B. T. Holland, C. F. Blanford and A. Stein, Mesoporous sieves with unified hybrid inorganic/organic frameworks, *Chem. Mater.*, 1999, **11**, 3302–3308.

4 E. Benson, A. Mehdi, V. Mansura, Y. Guari, C. Reyé and R. Corriú, One-step template-directed synthesis of multifunctionalised nanoporous silica: on the way to interactive nanomaterials, *Chem. Commun.*, 2005, 1775–1777.

5 E. Benson, A. Medí, C. Reyé and R. J. P. Corriú, Functionalisation of the framework of mesoporous organisilicas by rare-earth complexes, *J. Mater. Chem.*, 2006, **16**, 246–248.

6 M. Manuela Silva, V. de Zea Bermudez, L. D. Carlos, A. Passos de Almeida and M. J. Smith, Sol–gel processing and structural study of europium-doped hybrid materials, *J. Mater. Chem.*, 1999, **9**, 1735–1740.

7 R. Corriú, A. Mehdi, A., C. Reyé and C. Thieuleux, Control of coordination chemistry in both the framework and the pore channels of mesoporous hybrid materials, *New J. Chem.*, 2003, **27**, 905–908.

8 G. S. Ofelt, Structure of the f^6 configuration with application to rare earth ions, *J. Chem. Phys.*, 1963, **38**, 2171–2180.

9 D. Parker, Excitement in f block: structure, dynamics and function of nine-coordinate chiral lanthanide complexes in aqueous media, *Chem. Soc. Rev.*, 2004, **33**, 156–165.

10 D. Parker, R. Dickins, H. Puschmann, C. Crossland and J. Howard, Being excited by lanthanide coordination complexes: aqua species, chirality, excited-state chemistry, and exchange dynamics, *Chem. Rev.*, 2002, **102**, 1977–2010.

11 R. D. Peacock, The intensities of lanthanide f–f transitions, *Struct. Bonding*, 1975, **22**, 83–122.

12 J. Chen and P. R. Selvin, Synthesis of 7-amino-4-trifluoromethyl-2-(1*H*)-quinolinone and its use as an antenna molecule for the luminescent europium polyaminocarboxylates chelates, *J. Photochem. Photobiol., A*, 2000, **135**, 27–32.

13 P. Ge and P. R. Selvin, Carbostyril derivatives as antenna molecules for luminescent lanthanide chelates, *Bioconjugate Chem.*, 2004, **15**, 1088–1094.

14 G. Vereb, E. Jares-Erijman, P. R. Selvin and T. M. Jovin, Temporally and spectrally resolved imaging microscopy of lanthanide chelates, *Biophys. J.*, 1998, **74**, 2210–2222.

15 M. Li and P. R. Selvin, Luminescent polyaminocarboxylate chelates of terbium and europium: the effect of chelate structure, *J. Am. Chem. Soc.*, 1995, **117**, 8132–8138.

16 R. Reisfeld, E. Zigansky and M. Gaft, Europium probe for estimation of site symmetry in glass films, glasses and crystals, *Mol. Phys.*, 2004, **102**, 1319–1330.

17 V. Lavin, P. Baube, C. K. Jayasankar, I. R. Martín and V. D. Rodriguez, On the local structure of Eu_{3+} ions in oxyfluoride glasses. Comparison with fluoride and oxide glasses, *J. Chem. Phys.*, 2001, **115**, 10935–10944.

18 E. W. J. L. Oomen and A. M. A. van Dongen, Europium (III) in oxide glasses. Dependence of the emission spectrum upon composition, *J. Non-Cryst. Solids*, 1989, **111**, 205–213.

19 L. D. Carlos, R. A. Sá Ferreira, M. C. Gonçalves and V. De Zea Bermudez, Local coordination of Eu(III) in organic–inorganic amine functionalized hybrids, *J. Alloys Compd.*, 2004, **374**, 50–55.

20 F. S. Richardson, Terbium (III) and europium (III) ions as luminescent probes and stains for biomolecular systems, *Chem. Rev.*, 1982, **82**, 541–552.

21 J. Bruno, W. DeW. Horrocks and R. J. Zauhar, Europium (III) luminescence and tyrosine to terbium energy transfer studies of invertebrate (octopus) calmodulin, *Biochemistry*, 1992, **31**, 7016–7026.

22 D. Cronce, W. De and W. Horrocks, Probing the metal-binding sites of cod paralbumin using Eu(III) ion luminescence and diffusion-enhanced energy transfer, *Biochemistry*, 1992, **31**, 7963–7969.

23 J. Bünzli and C. Piguet, Lanthanide-containing molecular and supramolecular polymetallic functional assemblies, *Chem. Rev.*, 2002, **102**, 1897–1928.

24 G. Winsberg, B. J. Scott and G. D. Stucky, pH-Sensing with mesoporous thin films, *Chem. Commun.*, 2001, **1**, 119–120.

25 S. Blair, P. Lowe, C. E. Mathieu, D. Parker, P. Kanthi Senanayade and R. Kataky, Narrow-range optical pH sensor based on luminescent europium and terbium complexes immobilized in a sol–gel glass, *Inorg. Chem.*, 2001, **40**, 5860–5867.

26 M. Montalti, L. Prodi, N. Zaccheroni, L. Charbonniere, L. Douce and R. Ziessel, A luminescent anion sensor based on a europium hybrid complex, *J. Am. Chem. Soc.*, 2001, **123**, 12694–12695.

27 O. S. Wolfbeis, *Fiber Optic Chemical Sensors and Biosensors*, vol. I and II, CRC Press, Boca Raton, FL, USA, 1991.

28 E. Cho and F. Bright, Pin-printed chemical sensor arrays for the simultaneous multianalyte quantification, *Anal. Chem.*, 2002, **74**, 1462–1466.

29 G. W. Gokel, W. Leevy and M. Weber, Crown ethers: sensors for ions and molecular scaffolds for materials and biological models, *Chem. Rev.*, 2004, **104**, 2723–2750.

30 S. Hilderbrand, M. Lim and S. Lippard, Dirhodium tetracarboxylate scaffolds as reversible fluorescence-based nitric oxide sensors, *J. Am. Chem. Soc.*, 2004, **126**, 4972–4978.

31 D. T. McQuade, A. E. Pullen and A. E. Swager, Conjugated polymer-based chemical sensors, *Chem. Rev.*, 2000, **100**, 2537–2574.

32 C. J. Brinker, and G. W. Scherer, *Sol–Gel Science. The Physics and Chemistry of Sol-Gel Processing*, Ac. Press Inc., 1990.

33 R. Reisfeld, Prospects of sol–gel technology towards luminescent materials, *Opt. Mater.*, 2001, **16**, 1–7.

34 F. Embert, A. Mahdi, C. Reyé and R. J. P. Corriú, Synthesis and luminescent properties of monophasic organic-inorganic hybrid materials incorporating europium (III), *Chem. Mater.*, 2001, **13**, 4542–4549.

35 A.-C. Franville, D. Zambon and R. Mahiou, Luminescence behavior of sol–gel derived hybrid materials resulting from covalent grafting of a chromophore unit to different organically modified alkoxysilanes, *Chem. Mater.*, 2000, **12**, 428–435.

36 P. Liu, H. Li, Y. Wang, B. Liu, W. Zhang, Y. Wang, W. Yan, H. Zhang and U. Schubert, Europium complexes immobilization on titania *via* chemical modification of titanium alkoxide, *J. Mater. Chem.*, 2008, **18**, 735–737.

37 R. Hernandez, A.-C. Franville, P. Minoofar, B. Dunn and J. I. Zink, Controlled placement of luminescent molecules and polymers in mesostructured sol–gel thin films, *J. Am. Chem. Soc.*, 2001, **123**, 1248–1249.

38 A. Lobnik, N. Majcen, K. Niederreiter and G. Uray, Optical pH sensor based on the absorption of antenna generated europium luminescence by bromothymolblue in a sol–gel membrane, *Sens. Actuators, B*, 2001, **74**, 200–206.

39 N. A. J. Sommerdijk, A. Poppe, C. A. Gibson and J. D. Wright, Unexpected complexation behaviour of a sol–gel immobilised dye: the development of an optical copper (II) sensor, *J. Mater. Chem.*, 1998, **8**, 565–567.

40 J. D. Wright and N. A. C. Higginson, Effects of matrix variation on pH and Cu^{2+} sensing properties of sol–gel entrapped Eriochrome cyanine R, *J. Mater. Chem.*, 2004, **14**, 201–208.

41 M. A. Kessler, Determination of copper at ng mL^{-1}-levels based on quenching of the europium chelate luminescence, *Anal. Chim. Acta*, 1998, **364**, 125–129.

42 P. Brayshaw, J. C. G. Bünzli, P. Froidenaux, J. M. Harrowfield, Y. Kim and A. N. Sobolev, Synthetic, structural, and spectroscopic studies on solids containing tris(dipicolinato) rare earth anions and transition or main group metal cations, *Inorg. Chem.*, 1995, **34**, 2068–2076.

43 W. de W, Horrocks Jr., B. Holmquist and B. L. Vallee, Energy transfer between terbium (III) and cobalt (II) in thermolysin: a new class of metal–metal distance probes, *Proc. Natl. Acad. Sci. U. S. A.*, 1975, **72**, 4764–4768.

44 P. R. Selvin, T. M. Rana and J. E. Hearst, Luminescence resonance energy transfer, *J. Am. Chem. Soc.*, 1994, **116**, 6029–6030.

This journal is © The Royal Society of Chemistry and Owner Societies 2008

45 P. R. Selvin, The renaissance of fluorescence resonance energy transfer, *Nat. Struct. Biol.*, 2000, **7**, 730–734.
46 A. Beeby, I. M. Clarkson, R. S. Dickins, S. Faulkner, D. Parker, L. Royle, A. S. de Souza, J. A. Gareth Williams and M. J. Woods, Non-radiative deactivation of the excited states of europium, terbium and ytterbium complexes by proximate energy-matched OH, NH and CH oscillators: an improved luminescence method for establishing solution hydration states, *J. Chem. Soc., Perkin Trans. 2*, 1999, 493–503.
47 G. M. Murray, R. V. Sarrio and J. R. Peterson, The effects of hydration on the luminescence spectra of the trisodium tris(2,6-pyridenedicarboxylato) europium (III) compounds, *Inorg. Chim. Acta*, 1990, **176**, 233–240.
48 A.-C. Franville, R. Mahiou, D. Zambon and J.-C. Cousseins, Molecular design of luminescent organic–inorganic hybrid materials activated by europium (III) ions, *Solid State Sci.*, 2001, **3**, 211–222.
49 S. L. B. Lana and A. B. Seddon, X-Ray diffraction studies of sol-gel derived ORMOSILS based on combination of tetramethoxysilane and trimethoxysilane, *J. Sol–Gel Sci. Technol.*, 1998, **13**, 461–466.
50 H. Cui, J. Chen, H. Zhou and Y. Lu, Synthesis and infrared and fluorescence spectra of rare earth complexes with a new amide ligand, *Spectrochim. Acta, Part A*, 2007, **68**, 478–483.
51 W.-N. Wu, W.-B. Yuan, N. Tang, R.-D. Yang, L. Yan and Z.-H. Xu, Synthesis, characterizations and luminescent properties of three novel aryl amide type ligands and their lanthanide complexes, *Spectrochim. Acta, Part A*, 2006, **65**, 912–91.
52 M. Ocania, V. Fornés and C. J. Serna, The variability of the infrared powder spectrum of amorphous SiO₂, *J. Non-Cryst. Solids*, 1989, **107**, 187–192.
53 P. J. Innocenzi, Infrared spectroscopy of sol–gel derived silica-based films: a spectra-Stern–Volmerstructure overview, *J. Non-Cryst. Solids*, 2003, **316**, 309–319.
54 W. De W. Horrocks Jr. and D. R. Sudnick, Lanthanide ion probes of structure in biology. Laser-induced luminescence decay constants provide a direct measure of the number of metal-coordinated water molecules, *J. Am. Chem. Soc.*, 1979, **101**, 334–340.
55 R. A. Sá Ferreira, L. D. Carlos, R. R. Gonçalvez, S. J. L. Ribeiro and V. de Zea Bermudez, Energy-transfer mechanisms and emission quantum yields in Eu³⁺-based siloxane-poly(oxyethylene) nanohybrids, *Chem. Mater.*, 2001, **13**, 2991–2998.
56 P. Liu, H. Li, Y. Wang, B. Liu, W. Zhang, Y. Wang, W. Yan, H. Zhang and U. Schubert, Europium complexes immobilization on titania *via* chemical modification of titanium alkoxide, *J. Mater. Chem.*, 2008, **18**, 735–737.
57 J. R. Lakowicz, *Principles of Fluorescence Spectroscopy*, Plenum Press, New York, 2nd edn, 1999.
58 B. C. Barja, A. Remorino, M. J. Roberti and P. F. Aramendía, Luminescence quenching of europium(III) and terbium(III) carboxylates by transition metals in solution, *J. Argent. Chem. Soc.*, 2005, **93**, 81–96.
59 S. Sherwin Lehrer, Solute perturbation of protein fluorescence. Quenching of the tryptophyl fluorescence of model compounds and of lysozyme by iodide ion, *Biochemistry*, 1971, **10**, 3254–3263.
60 E. R. Carraway, J. N. Demas and B. A. DeGraff, Luminescence quenching mechanism for microheterogeneous systems, *Anal. Chem.*, 1991, **63**, 332–336.
61 I. Grenthe, Stability relationships among the rare earth dipicolinates, *J. Am. Chem. Soc.*, 1961, **83**, 360–364.
62 M. C. Burleigh, M. A. Markowitz, M. S. Spector and B. P. Gaber, Amine-functionalized periodic mesoporous organosilica, *Chem. Mater.*, 2001, **13**, 4760–4766.
63 A. Walcarius, M. Etienne and B. Lebeau, Rate of access to the binding sites in organically modified silicates. 2. Ordered mesoporous silicas grafted with amine or thiol groups, *Chem. Mater.*, 2003, **15**, 2161–2173.
64 B. C. Barja, A. Remorino and P. F. Aramendia, Luminescence quenching of Eu(III) carboxylates by Cu(II) in a composite polymer xerogel film, *J. Photochem. Photobiol., A*, 2005, **82**, 43–49.